Nano Res. 2011, 4(3): 290–296
DOI 10.1007/s12274-010-0081-x
Research Article

ISSN 1998-0124
CN 11-5974/O4

Hybrid Silicon-Carbon Nanostructured Composites as Superior Anodes for Lithium Ion Batteries

Po-Chiang Chen[1], Jing Xu[1], Haitian Chen[2], and Chongwu Zhou[2] (✉)

[1] Mork Family Department of Chemical Engineering and Materials Science, University of Southern California, Los Angeles, CA 90089, USA
[2] Ming-Hsieh Department of Electrical Engineering, University of Southern California, Los Angeles, CA 90089, USA

Received: 6 October 2010 / Revised: 13 November 2010 / Accepted: 13 November 2010

ABSTRACT

We have successfully fabricated a hybrid silicon–carbon nanostructured composite with large area (about 25.5 in^2) in a simple fashion using a conventional sputtering system. When used as the anode in lithium ion batteries, the uniformly deposited amorphous silicon (a-Si) works as the active material to store electrical energy, and the pre-coated carbon nanofibers (CNFs) serve as both the electron conducting pathway and a strain/stress relaxation layer for the sputtered a-Si layers during the intercalation process of lithium ions. As a result, the as-fabricated lithium ion batteries, with deposited a-Si thicknesses of 200 nm or 300 nm, not only exhibit a high specific capacity of >2000 mA·h/g, but also show a good capacity retention of over 80% and Coulombic efficiency of >98% after a large number of charge/discharge experiments. Our approach offers an efficient and scalable method to obtain silicon–carbon nanostructured composites for application in lithium ion batteries.

KEYWORDS

Amorphous silicon, carbon nanofibers, lithium ion batteries, hybrid nanostructured composite

1. Introduction

In recent years, due to the depletion of fossil fuels and the increasing concern about environmental issues, interest in developing alternative energy sources and devices, including solar cells, fuel cells, supercapacitors, and lithium ion batteries, has increased rapidly [1–6]. Among the above-mentioned energy conversion and storage devices, lithium ion batteries have been widely applied in both portable electronics and consumer electronics because of their high energy density, high power density, and low fabrication cost. Most research efforts have been devoted to the synthesis of electrode materials and the design of electrode structures [7, 8] by adapting nanostructured materials. One-dimensional (1-D) nanostructures, have the advantages of high surface area (such as single-walled carbon nanotubes with a surface area of 300–600 m^2/g) and short ion diffusion length, and have been viewed as components for next-generation electrochemical energy conversion and storage devices [9–11]. For instance, TiO_2–B nanowires have been shown to have a higher specific capacity than TiO_2–B nanoparticle-based materials when used as anodes in lithium ion batteries [11].

More recently, silicon (Si) nanostructures have been suggested to be one of the most promising anode materials for lithium ion batteries and have attracted considerable attention because of their large theoretical gravimetric specific capacity of 4200 mA·h/g and relatively low working potential at around 0.5 V vs.

Address correspondence to chongwuz@usc.edu

Li/Li$^+$ [12–20]. For instance, Chan et al. reported Si nanowires as anode materials and successfully demonstrated an excellent specific capacity of 3124 mA·h/g during the first discharge process [12]. Further developments include using homogeneous Si nanowires and hybrid Si core–shell nanowires, which have been demonstrated to deliver superior device performance as battery electrodes [21, 22]. For example, $TiSi_2$–Si core–shell nanowires have been reported as one example of such novel Si nanostructure-based anodes [21]. The highly conductive core $TiSi_2$ nanowires provide the electron conducting pathway and improve the battery power density by a factor of two. The $TiSi_2$ nanowires also serve as a mechanical support and release the structural stress/strain associated with lithium ion insertion/extraction processes. In addition to core–shell nanowires, the preparation of nanostructured carbon–silicon composites seems to be another promising approach to solve the capacity retention problem [23–26]. However, synthesis of the above-mentioned materials usually requires a high temperature chemical vapor deposition process, and therefore alternative methods that can avoid a high-temperature process would be very interesting and attractive.

In this paper, we present a rather simple but efficient approach to obtain hybrid Si-based nanostructured composites. By simply using a conventional sputtering system to deposit amorphous silicon (a-Si) on carbonaceous materials pre-deposited on copper foil, we are able to obtain a hybrid Si-based nanostructured composite with a large area of 25.5 in^2 and employ it as an anode in lithium ion batteries. In our design, carbon nanofibers (CNFs) are used as both mechanical support and electron conducting pathway. Different thicknesses of sputtered silicon were deposited on pre-deposited carbonaceous materials as the active materials to store electrical energy, as illustrated in Fig. 1(a). These hybrid Si-based nanostructured electrodes (Si/CNF) exhibit a high charge storage capacity of ~2528 mA·h/g and good cycling life up to a large number of charge/discharge cycles (>105 cycles). In addition, the as-fabricated batteries also show a Coulombic efficiency of 88% in the first cycle and over 98% in the following cycles, which are comparable with results in the literature [25–28].

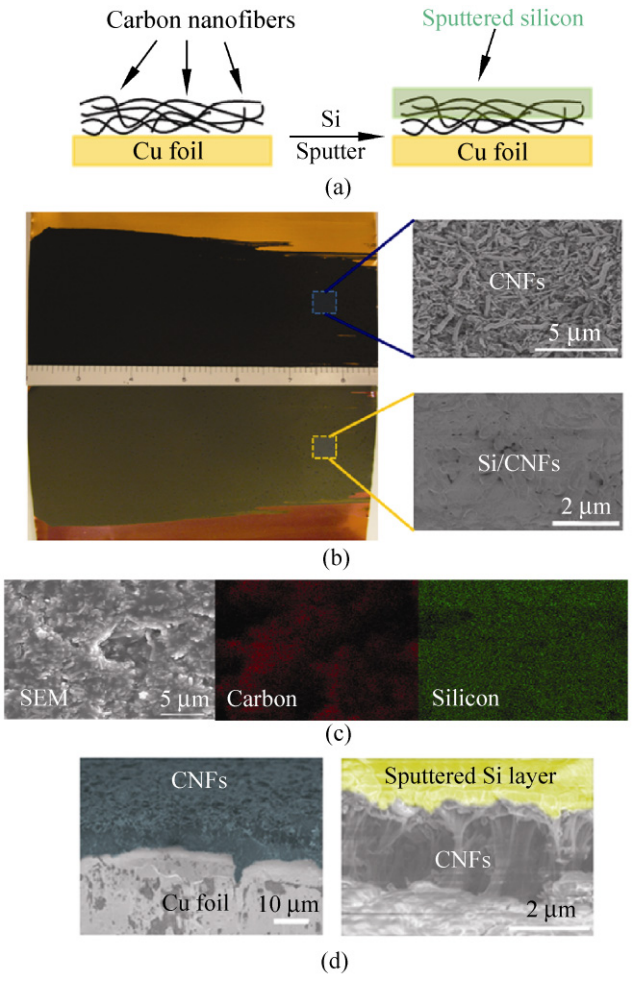

Figure 1 (a) Schematic diagram of sputtered silicon on CNF/copper foil. (b) Photographs of CNFs on a copper foil before and after 200 nm silicon deposition. (c) Top-view SEM and EDX images of sputtered Si on CNFs. (d) Side-view of CNFs before and after 500 nm silicon deposition

2. Experimental

The fabrication of Si hybrid nanostructured thin film electrodes began with the preparation of a CNF film on copper foil. CNFs (Sigma-Aldrich) were deposited on copper (Cu) foil via a so-called slurry spreading method, which has been widely adopted in the preparation of lithium ion battery electrodes. In brief, CNFs were mixed with polyvinylidene fluoride (PVDF, 10 wt%) in *N*-methylpyrrolidone (NMP) to form a uniform slurry, and then spread onto a copper foil using a stainless steel blade. The samples were installed in a conventional sputtering system (Denton Discovery Sputtering System) for Si deposition. The loading

density of as-prepared CNF films was about 0.4 mg/cm^2 on average.

Silicon deposition on CNFs was carried out in an argon (Ar)-filled environment at room temperature, with a deposition rate of 6 nm/min and varied deposition thicknesses of 100 nm, 200 nm, 300 nm, or 500 nm. In order to compare the sputtered Si/CNF anodes and Si electrodes, we sputtered 200 nm Si directly on to a Cu foil as the reference sample. The as-prepared samples were then characterized by field-emission scanning electron microscopy (FE-SEM, Hitachi S-4800) and energy-dispersive X-ray spectroscopy (EDS, Jeol, JSM-7001F). CR2032 coin cells were assembled in an Ar-filled glove box by using the as-prepared Si/CNF anode as the working electrode and lithium metal foil as the counter electrode. The electrolyte was 1 mol/L $LiClO_4$ dissolved in a 1:1 (weight ratio) mixture of ethylene carbonate (EC) and diethyl carbonate (DEC).

3. Results and discussion

Figure 1(b) displays a photograph of a typical CNF film on a Cu foil before (upper image) and after (lower image) the deposition of 500 nm Si. The Si sputtered area is about 8.5 in × 3 in, making this method a more efficient way to prepare large area Si-based electrodes than the chemical vapor deposition (CVD) processes previously employed to prepare CNF-amorphous Si core–shell nanowire or Si nanowire anodes [12, 22]. The zoomed-in SEM images in Fig. 1(b) are the top-view SEM images before and after the Si deposition. A uniform pre-deposited CNF thin film on a the Cu foil can be clearly observed before Si deposition. After Si deposition, the CNFs were fully covered by a continuous Si film forming a hybrid Si/CNF nanostructured thin film electrode. In order to study the interface between the CNFs and the sputtered Si layer, we intentionally stretched a Si/CNF hybrid film electrode. In the top-view SEM image, shown in Fig. 1(c), a uniform layered structure of a sputtered Si layer and CNFs can be clearly identified by the contrast in the image. The thickness of the sputtered Si layer shown in Fig. 1(c) is about 500 nm. Fig. 1(d) shows side-view SEM images of the electrodes before and after silicon sputtering with artificial colors used to distinguish between carbon nanofibers (green) and sputtered silicon (yellow). It can be seen that sputtered Si forms a uniform coating on CNFs, which is consistent with the image in Fig. 1(c).

Electrochemical measurements of sputtered Si/CNF anodes were carried out with a battery testing system (MSTAT, Arbin) and a potentiostat (Gamry Reference 600). The cyclic voltammetry (CV) profiles of sputtered Si/CNF anodes were obtained using the Si/CNF electrode as the working electrode and Li foil as the reference electrode. Figure 2(a) shows the first three CV curves of a sputtered Si/CNF anode with a deposited Si thickness of 200 nm, in a potential window between 0.01 V and 3.0 V, with a scan rate of 0.05 mV/s. Two pairs of signature redox peaks of amorphous Si can be found at around 0.18/0.03 V (reduction) and 0.50/0.30 V (oxidation) in the first cycling curve (blue line), which indicates the occurrence of Si–Li reactions in the sputtered Si/CNF anode [28]. The shape of the first cycling curve differs from that of the second and third curves, where the sharp peak at 0.18 V disappears and the peaks at 0.50/0.30 V shift towards a lower potential. The irreversible reaction in the first cycle can be attributed to the formation of a solid electrolyte interface (SEI) layer or a phase transformation [29]. However, the second and the third cycles match almost exactly, which implies the system has reached a steady state. No significant peaks related to CNFs [30] can be observed in Fig. 2(a). Overall, our sputtered Si/CNF anodes display CV characteristics similar to amorphous silicon [28], but different from carbon nanofibers [30], suggesting the redox behavior of our anodes is dominated by the sputtered Si layer rather than the pre-coated CNF thin films.

Galvanostatic (GV) charge/discharge measurements were used to determine the specific capacity (C_{sp}), and the Coulombic efficiency of the devices in a two-electrode configuration. Figure 2(b) shows the cycling performance of a 200 nm sputtered Si/CNF anode up to 95 cycles, with a constant charge/discharge current of 0.05 A/g. In the initial state, the potential dropped to 0.22 V and maintained a flat plateau at around ~0.25 V, before gradually decreasing to 0.01 V. The stepped behavior of the discharge potential may result from the inactive nature of the Si film in the electrochemical reactions [29]. The capacity in the

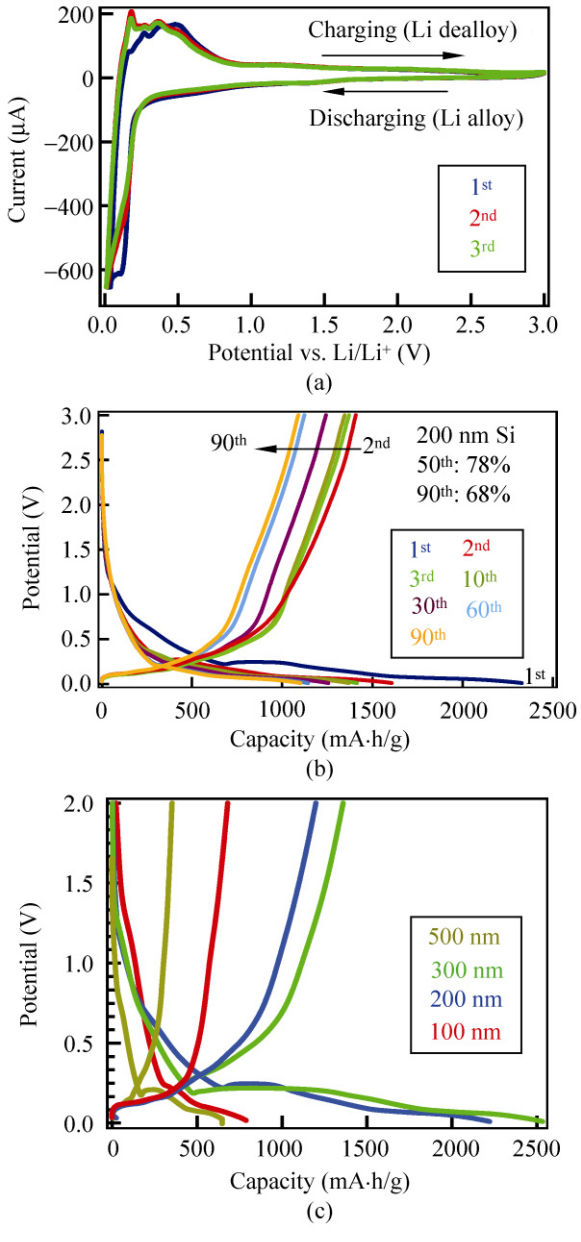

Figure 2 (a) Cyclic voltammograms for 200 nm Si on CNFs from 0.01 to 3.0 V. The first three cycles are shown. (b) Voltage profile for first 90 cycles of the 200 nm sputtered Si/CNF anode at a constant charge/discharge current of 0.05 A/g. (c) Voltage profile for the first cycle of the 100 nm, 200 nm, 300 nm, and 500 nm Si/CNF anodes at a constant charge/discharge current of 0.05 A/g

first discharge process of sputtered Si/CNF anodes was about 2320 mA·h/g. Our results are better than those reported for an amorphous Si microbattery (~650 mA·h/g), and close to those reported for CNF–amorphous Si core–shell nanostructured electrodes. In addition, the Coulombic efficiency of our devices in the first cycle is about 88%, which is comparable to that of commercial graphite anodes (~90%) and better than that of lithium ion batteries made of single-crystalline Si nanowires (~73%) [22]. The second discharge capacity decreased to 1608 mA·h/g, which can be attributed to the irreversible nature of Li–Si insertion and the formation of an SEI layer. After the first cycle, the reversible charge/discharge reactions were maintained over the subsequent 80 cycles.

To further understand the GV behavior of sputtered Si/CNF anodes, we prepared Si/CNF anodes with different sputtering Si thicknesses of 100 nm, 300 nm, and 500 nm, and then performed GV measurements with the resulting Si/CNF anodes using a constant charge/discharge current of 0.05 A/g. The Si weight loadings were 5.8%, 15.5%, and 23.6% for 100 nm, 300 nm, and 500 nm sputtered Si, respectively. The first cycle for the Si/CNF anodes can be found in Fig. 2(c). As one can see, the voltage profile of 100 nm sputtered Si/CNF anode is quite different from that of 200 nm, 300 nm, and 500 nm sputtered Si/CNF anodes. The plateau at 0.22 V is short and not easy to observe, which indicates the discharge capacity might be contributed by the CNFs underneath the 100 nm sputtered Si, and the discharge capacity is only 786 mA·h/g. On the other hand, with more Si deposition on the CNFs, both 300 nm and 500 nm sputtered Si/CNF anodes exhibit prolonged plateaus at around 0.22 V. The 300 nm sputtered Si/CNF anode shows the highest discharge capacity of 2528 mA·h/g, which is more than three-times that of the 100 nm sputtered Si/CNF anode. However, the discharge capacity of 500 nm sputtered Si/CNF anode is only 648 mA·h/g. In conclusion, our observations indicate that 200 nm and 300 nm films offer better performance than 500 nm films. More experiments are required to understand these phenomena.

Figure 3(a) shows plots of the capacity retention versus cycling number for electrodes with different thicknesses of sputtered Si (100 nm, 200 nm, and 300 nm). The weight densities for 100 nm, 200 nm and 300 nm sputtered Si are 0.02 mg/cm^2, 0.049 mg/cm^2 and 0.071 mg/cm^2, respectively. When calculating the capacity, we have included the weight of the CNFs. As one can see, all Si/CNF anodes displayed good capacity retention, especially the 100 nm Si/CNF anode (~84% after 95 cycles). This is probably because there

is more space for volume expansion than in the thicker sputtered Si samples. For 200 nm Si/CNF anodes, the capacity retention up to the 50th cycle (~80%) is close to values reported in the literature. Good capacity retention was also observed even at a higher charge/discharge rate (*C*/4). In this case, as shown in Fig. 3(b), the 300 nm Si/CNF anode exhibited a high specific capacity up to 1200 mA·h/g after 105 cycles, corresponding to over 90% capacity retention. In the initial stage of the cycle tests, a reduced capacity was observed, and after about 10 cycles, the capacity recovered to about 1200 mA·h/g. Similar observations have reported by Takamura et al. [31, 32] and can be understood in terms of the Si film initially being very compact and unable to accept a large amount of Li, but after repeated Li insertion/extraction, the film structure underwent changes enabling it to accept more Li. To highlight the advantage of our Si/CNF anodes, we directly sputtered 200 nm Si on Cu foil (Si/Cu) and carried out GV measurements as a comparison. As expected, the Si/Cu anode showed extremely poor capacity retention, which can be attributed to the huge volume expansion after Li ion insertion/extraction. After 20 cycles, there was almost no measurable capacity from the anode, indicating a total loss of active material. We also investigated the Coulombic efficiency of our devices and, as an example, the results for the 200 nm sputtered Si/CNF anodes are shown in Fig. 3(c). The cell exhibited a good first cycle of Coulombic efficiency of 88%. The Coulombic efficiency in the second cycle increased to 93% and a very high Coulombic efficiency between 98%–99% was maintained over the next 80 cycles. Subsequently, the discharge capacities faded a little but remained at ~70% up to 90 cycles (relative to the second cycle). Such good capacity retention was not observed for the 200 nm electrode, but also for 100 nm and 300 nm sputtered Si/CNF anodes.

In order to study any variation in chemical composition of our sputtered Si/CNF anodes after the cycling experiments, EDS was carried out and the results are shown in Fig. 4. The SEM image of a 200 nm sputtered Si/CNF anode after 95 charge/discharge cycles (Fig. 4(a)) clearly shows that there is still good adhesion between Si and the substrate. In addition, compared with the pristine surface shown in Fig. 1(b),

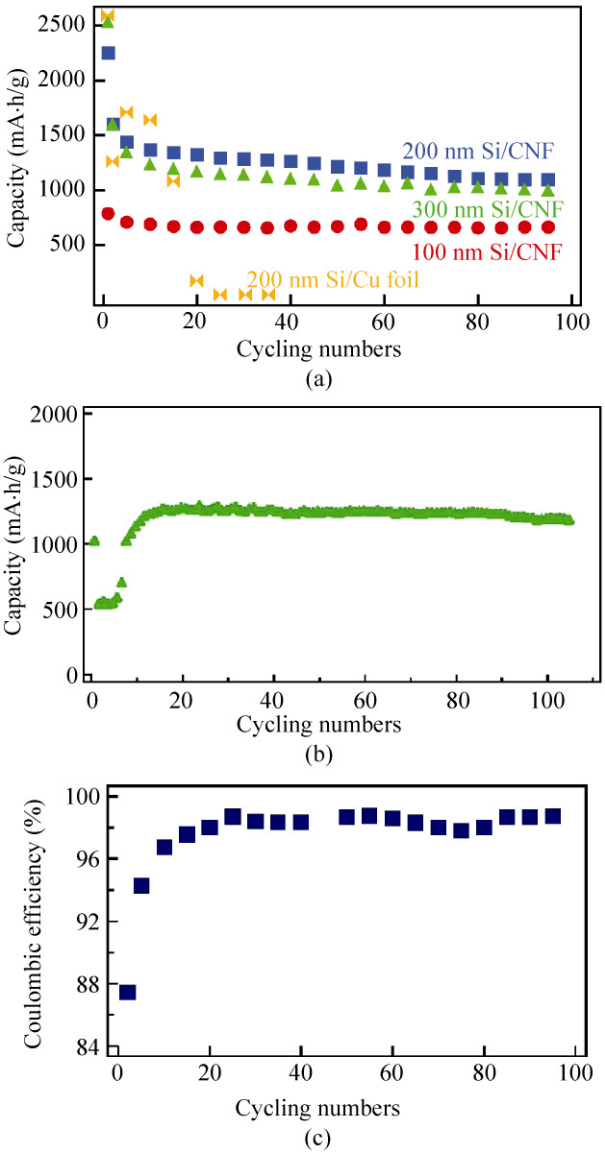

Figure 3 (a) Discharge capacity of 100 nm, 200 nm, and 300 nm sputtered Si/CNF anodes, and 200 nm Si/Cu anodes at a current rate *C*/10. (b) Discharge capacity of 300 nm sputtered Si/CNF anodes at a current rate *C*/4. (c) Coulombic efficiency of a 200 nm sputtered Si/CNF anode

the Si surface after 95 cycles appears rough, as a consequence of the lithiation/delithiation processes. Figures 4(b) and 4(c) show EDS images of the sputtered Si/CNF electrodes. The red color represents carbon atoms and the green color indicates the presence of silicon atoms. The EDS mapping strongly suggests that the sputtered Si layer is still well coated on CNFs and has a strong adhesion with them, even after a large number of cycling experiments. Although the sputtered Si film was broken into small grain domains

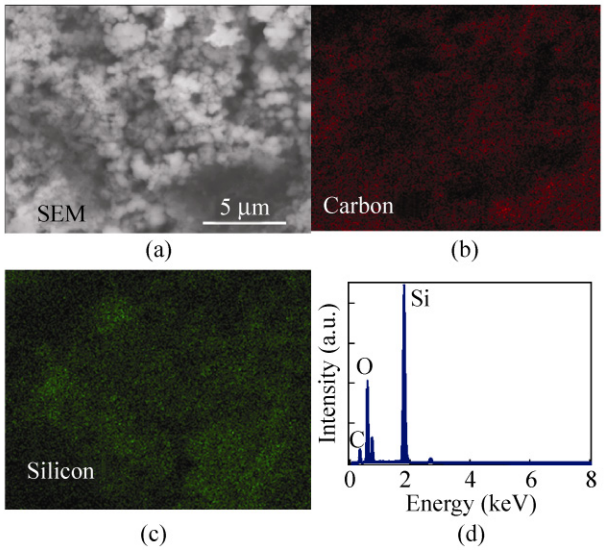

Figure 4 (a) SEM image of 200 nm sputtered Si/CNF anodes after 95 cycles of charge/discharge measurements. (b) EDS image of carbon atoms. (c) EDS image of silicon atoms. (d) EDS spectrum of 200 nm sputtered Si/CNF anodes after 95 cycles of chargeg/dischare measurements

after lithiation/delithiation processes, as shown in Fig. 4(c), the good capacity retention and the EDS results indicate that each grain domain maintained its strong adhesion with the underlying CNFs. A similar observation was recently reported by Rong et al. [33], who concluded that a Si film can form a convex morphology with a cone-shaped "lattice" on the surface which can be squeezed to release the internal stress. Figure 4(d) shows a typical EDS spectrum of the sputtered Si/CNF electrodes. The atomic ratio of C:Si is estimated to be 9:1.

4. Conclusions

We have developed a simple and efficient way to obtain hybrid nanostructured thin film electrodes for use in lithium ion batteries. Our hybrid nanostructured Si/CNF anodes exhibited superior device performance to those for materials used in previous studies, in terms of both specific capacity and cycle life. The superior performance can be attributed to (1) the utilization of CNFs, which provide a good strain/stress relaxation layer and a conductive electron pathway, and (2) the sputtered amorphous Si, which contributes high specific capacity to the half cells. In addition, compared to conventional batteries, the total weight of our devices is reduced because binder materials are not required. Si/CNF lithium ion batteries are expected to find applications in portable electronics and electrical vehicles.

Acknowledgements

We acknowledge financial support from the National Science Foundation (CCF 0726815 and CCF 0702204).

References

[1] Winter, M.; Brodd, R. J. What are batteries, fuel cells, and supercapacitors. *Chem. Rev.* **2004**, *104*, 4245–4270.

[2] Kang, K.; Meng, Y. S.; Bréger, J.; Grey, C. P.; Ceder, G. Electrodes with high power and high capacity for rechargeable lithium batteries. *Science* **2006**, *311*, 977–980.

[3] Yoon, J.; Baca, A. J.; Park, S. -I.; Elvikis, P.; Geddes, J. B., Ⅲ; Li, L.; Kim, R. H.; Xiao, J.; Wang, S.; Kim, T. -H.; Motala, M. J.; Ahn, B. Y.; Duoss, E. B.; Lewis, J. A.; Nuzzo, R. G.; Ferreira, P. M.; Huang, Y.; Rockett, A.; Rogers, J. A. Ultrathinsilicon solar microcells for semitransparent, mechanically flexible and microconcentratormoduledesigns. *Nat. Mater.* **2008**, *7*, 907–915.

[4] Armand, M.; Tarascon, J. -M. Building better batteries. *Nature* **2008**, *451*, 652–657.

[5] Boettcher, S. W.; Spurgeon, J. M.; Putnam, M. C.; Warren, E. L.; Turner-Evans, D. B.; Kelzenberg, M. D.; Maiolo J. R.; Awater, H. A.; Lewis, N. S. Energy-conversion properties of vapor–liquid–solid-grown silicon wire-array photocathodes. *Science* **2010**, *327*, 185–187.

[6] Long, J. W.; Dunn, B.; Rolison, D. R.; White, H. S. Three-dimensional battery architectures. *Chem. Rev.* **2004**, *104*, 4463–4492.

[7] Liu, J.; Cao, G.; Yang, Z.; Wang, D.; Dubois, D.; Zhou, X.; Graff, G. L.; Pederson, L. R.; Zhang, J. -G. Oriented nanostructures for energy conversion and storage. *ChemSusChem* **2008**, *1*, 676–697.

[8] Simon, P.; Gogotsi, Y. Materials for electrochemical capacitors. *Nat. Mater.* **2008**, *7*, 845–854.

[9] Jiang, C.; Hosono, E.; Zhou, H. E. Nanomaterials for lithium ion batteries. *Nano Today* **2006**, 1, 28–33.

[10] Poizot. P.; Laruelle, S.; Grugeon, S.; Dupont, L.; Tarascon, T. -M. Nano-sized transition-metal oxides as negative-electrode materials for lithium-ion batteries. *Nature* **2000**, *407*, 496–499.

[11] Arico, A. S.; Bruce, P.; Scrosati, B.; Tarascon, T. -M.; Schalkwijk, W. V. Nanostructured materials for advanced

energy conversion and storage devices. *Nat. Mater.* **2005**, *4*, 366–377.

[12] Chan, C. K.; Peng, H.; Liu, G.; Mcilwrath, K.; Zhang, X. F.; Huggins, R. A.; Cui, Y. High-performance lithium battery anodes using silicon nanowires. *Nat. Nanotechnol*. **2008**, *3*, 31–35.

[13] Park, M. H.; Kim, M. G.; Joo, J.; Kim, K.; Kim, J.; Ahn, S.; Cui, Y.; Cho, J. Silicon nanotube battery anodes. *Nano Lett*. **2009**, *9*, 3844–3847.

[14] Song, T.; Xia, J.; Lee J. -H.; Lee, D. H.; Kwon, M. -S.; Choi, J. -M.; Wu, J.; Doo, S. K.; Chang, H.; Park, W. I.; Zang, D. S.; Kim, H.; Huang, Y.; Hwang, K. -C.; Rogers, J. A.; Paik, U. Arrays of sealed silicon nanotubes as anodes for lithium ion batteries. *Nano Lett*. **2010**, *10*, 1710–1716.

[15] Cho, J. Porous Si anode materials for lithium rechargeable batteries. *J. Mater. Chem.* **2010**, *20*, 4009–4014.

[16] Kim, H.; Han, B.; Choo J.; Cho, J. Three-dimensional porous silicon particles for use in high-performance lithium secondary batteries. *Angew. Chem. Int. Ed.* **2008**, *47*, 10151–10154.

[17] Kim, H.; Cho, J. Superior lithium electroactive mesoporous Si@carbon core–shell nanowires for lithium battery anode material. *Nano Lett.* **2008**, *8*, 3688–3691

[18] Kim, H; Seo, M.; Park, M. -H.; Cho, J. A critical size of silicon nano-anodes for lithium rechargeable batteries. *Angew. Chem. Int. Ed.* **2010**, *49*, 2146–2149.

[19] Cui, L. F.; Hu, L. B.; Choi, J. K.; Cui, Y. Light-weight free-standing carbon nanotube–silicon films for anodes of lithium ion batteries. *ACS Nano* **2010**, *4*, 3671–3678

[20] Choi, J. W.; Hu, L. B.; Cui, L. F.; McDonough, J. R.; Cui, Y. Metal current collector-free freestanding silicon-carbon 1D nanocomposites for ultralight anodes in lithium ion batteries. *J. Power Sources* **2010**, *195*, 8311–8316

[21] Zhou, S.; Liu, Z.; Wang, D. Si/$TiSi_2$ heteronanostructures as high-capacity anode material for Li ion batteries. *Nano Lett*. **2010**, *10*, 860–863.

[22] Cui, L. F.; Yang, Y.; Hsu, C. M.; Cui, Y. Carbon–silicon core–shell nanowires as high capacity electrode for lithium ion batteries. *Nano Lett*. **2009**, *9*, 3370–3374.

[23] Wang, L.; Ding, C. X.; Zhang, L. C.; Xu, H. W.; Zhang, D. W.; Cheng, T.; Chen, C. H. A novel carbon–silicon composite nanofiber prepared via electrospinning as anode material for high energy-density lithium ion batteries. *J. Power Sources* **2010**, *195*, 5052–5056.

[24] Wang, W.; Kumta, P. N. Nanostructured hybrid silicon/carbon nanotube heterostructures: Reversible high-capacity lithium-ion anodes. *ACS Nano* **2010**, *4*, 2233–2241.

[25] Luo, Z.; Fan, D.; Liu, X.; Mao, H.; Yao, C.; Deng, Z. High performance silicon carbon composite anode materials for lithium ion batteries. *J. Power Sources* **2009**, *189*, 16–21.

[26] Saint, J.; Morcrette, M.; Larcher, D.; Laffont, L.; Beattie, S.; Peres, J. -P.; Talaga, D.; Couzi, M.; Tarascon, J. -M. Towards a fundamental understanding of the improved electrochemical performance of silicon–carbon composites. *Adv. Funct. Mater*. **2007**, *17*, 1765–1774.

[27] Cui, L. F.; Ruffo, R.; Chan, C. K.; Peng, H. L.; Cui, Y. Crystalline-amorphous core–shell silicon nanowires for high capacity and high current battery electrodes. *Nano Lett.* **2009**, *9*, 491–495.

[28] Baranchugov, V.; Markevich, E.; Pollak, E.; Salitra, G.; Aurbach, D. Amorphous silicon thin films as a high capacity anodes for Li-ion batteries in ionic liquid electrolytes. *Electrochem. Commun.* **2007**, *9*, 796–800.

[29] Lee, K. -L.; Jung, J. -Y.; Lee, S. -W.; Moon, H. -S.; Park, J. -W. Electrochemical characteristics and cycle performance of $LiMn_2O_4$/a-Si microbattery. *J. Power Sources* **2004**, *130*, 241–261.

[30] Zaghib, K.; Tatsumi, K.; Abe, H.; Ohsaki, T.; Sawada, Y.; Higuchi, S. Optimization of the dimensions of vapor-grown carbon fiber for use as negative electrodes in lithium-ion rechargeable cells. *J. Electrochem. Soc.* **1998**, *145*, 210–215.

[31] Takamura, T.; Ohara, S.; Uehar, M.; Suzuki, J.; Sekine, K. A vacuum deposited Si film having a Li extraction capacity over 2000 mA·h/g with a long cycle life. *J. Power Sources* **2004**, *129*, 96–100.

[32] Ohara, S.; Suzuki, J.; Sekine, K.; Takamura, T. A thin film silicon anode for Li-ion batteries having a very large specific capacity and long cycle life. *J. Power Sources* **2004**, *136*, 303–306.

[33] Rong, J. P.; Masarapu, C.; Ni, J.; Zhang, Z. J.; Wei, B. Q. Tandem structure of porous silicon film on single-walled carbon nanotube macrofilms for lithium-ion battery applications. *ACS Nano* **2010**, 4, 4683–4690.